Published in "Physical Review B 88(12): 125126, 2013"
which should be cited to refer to this work.

Ordered phases in the Holstein-Hubbard model: Interplay of strong Coulomb interaction and electron-phonon coupling

Yuta Murakami,[1] Philipp Werner,[2] Naoto Tsuji,[1] and Hideo Aoki[1]
[1]*Department of Physics, University of Tokyo, Hongo, Tokyo 113-0033, Japan*
[2]*Department of Physics, University of Fribourg, 1700 Fribourg, Switzerland*

We study the Holstein-Hubbard model at half filling to explore ordered phases including superconductivity (SC), antiferromagnetism (AF), and charge order (CO) in situations where the electron-electron and electron-phonon interactions are strong (comparable to the electronic bandwidth). The model is solved in the dynamical mean-field approximation with a continuous-time quantum Monte Carlo impurity solver. We determine the superconducting transition temperature T_c and the SC order parameter and show that the phonon-induced retardation or the strong Coulomb interaction leads to a significant reduction and shift of the T_c dome against the effective electron-electron interaction $U_{\rm eff}$ given by the Hubbard U reduced by the phonon-mediated attraction in the static limit. This behavior is analyzed by comparison to an effective static model in the polaron representation with a renormalized bandwidth. In addition, we discuss the superconducting gap Δ and $2\Delta/T_c$ to reveal the effect of the retardation and the Coulomb interaction. We also determine the finite-temperature phase diagram including AF and CO. In the moderate-coupling regime, there is a hysteretic region of AF and CO around $U_{\rm eff} = 0$, while the two phases are separated by a paramagnetic metal in the weak-coupling regime and a paramagnetic insulator in the strong-coupling regime.

I. INTRODUCTION

While the physics of correlated electron systems is an interesting and formidable problem in its own right, several classes of interesting materials exhibit an interplay of strong electron-electron Coulomb repulsion and strong electron-phonon coupling. For example, the electron-phonon coupling in high-T_c cuprates is strong, as evidenced by the kinks observed in the angle-resolved photoemission spectrum.[1] In alkali-doped fullerides an s-wave superconducting phase borders an antiferromagnetic phase in the temperature-pressure phase diagram,[2–4] and the transition temperature of the superconducting state has recently been found to be dome shaped. These features indicate that in these classes of materials, both the electron-electron Coulomb repulsion and the electron-phonon interaction are strong. Likewise, in aromatic superconductors such as picene (a recent addition to carbon-based materials), the electron-electron and electron-phonon interactions are reported to be strong,[5–9] although the mechanism of superconductivity in the aromatic compounds is still totally unclear. Correlated electron systems often provide an interesting arena in which various phases compete with each other. In the presence of strong electron-electron and electron-phonon interactions, the problem should become even richer.

The Holstein-Hubbard (HH) model is a simple model which allows us to describe and explore the interplay of electron-electron and electron-phonon interactions. The model incorporates a coupling between electrons and dispersionless (i.e., Einstein) phonons with energy ω_0, in addition to the on-site Hubbard interaction U. There is a body of works which investigates the competition between the two interactions in this model. The study of the one-dimensional case based on the density matrix renormalization group (DMRG) technique or quantum Monte Carlo analysis has revealed some general features.[10–12] However, since ordered phases with continuous symmetry breaking do not occur in $D = 1$, it is difficult to elucidate the generic behavior of ordered states from these calculations, although we can indeed discuss quasiordered states in terms of the Tomonaga-Luttinger picture. In $D = 2$, several works on this model have revealed interesting properties caused by the coexistence of two types of interactions.[13–17] In the opposite limit of infinite spatial dimensions, $D = \infty$, where the dynamical mean-field theory (DMFT) becomes exact,[18–20] ordered states with full symmetry breaking exist even at nonzero temperature, and analyses in this dimension provide further insights into the effect of these competing interactions. The symmetric phases have been studied in Refs. 21–24, and the corresponding phase diagram has been determined.

As for the ordered states, their properties have been investigated in several works,[25–29] but many issues remain unresolved. The ground-state phase diagram around $U = \lambda$, where λ is the static effective electron-electron interaction mediated by the phonons, has been determined in Refs. 26 and 27, and the accuracy of and deviations from the conventional theory[30–33] of superconductivity have been discussed.[28,29] An important issue is the following: the electron-phonon coupled system is often regarded as having an effective interaction $U_{\rm eff} \equiv U - \lambda$, but this is only strictly valid in the antiadiabatic limit for the phonon energy, $\omega_0 \to \infty$, where the interaction in the HH model becomes nonretarded, and the real question is to what extent this approximation remains valid when we vary U and/or ω_0. In other words, for a finite ω_0 the phonon-mediated interaction is certainly retarded, and for a small enough phonon frequency, the static model with $U_{\rm eff}$ can be expected to fail. Thus the nature of the superconducting

state in the regime where U, λ, and ω_0 are all comparable to the bandwidth W poses a challenging problem, which is not only conceptually interesting but may have relevance to real materials with strong electron-electron and electron-phonon interactions. The problem, however, has not been properly understood since superconducting states in such a regime cannot be treated within conventional theories such as the Migdal-Eliashberg theorem[30,31] or the McMillan equation.[33] Another open issue is the finite-temperature phase diagram for ordered phases in the vicinity of $U = \lambda$.

With these questions in mind, we study in this paper ordered states in the half-filled Holstein-Hubbard model to clarify the effect of the coexistence of electron-electron and electron-phonon interactions on the s-wave superconducting state (SC), the antiferromagnetic (AF) state, and the charge-ordered state (CO). In our study we employ DMFT, with a continuous-time quantum Monte Carlo (CT-QMC) impurity solver, which is exact up to statistical errors and can, in principle, access any parameter regime down to temperatures of about 1% of the electronic bandwidth. Furthermore, in principle, DMFT + CT-QMC can treat these three ordered states without bias, which enables us to systematically investigate their competition in the regime where U, λ, and ω_0 are comparable to the bandwidth. While there have been several works discussing ordered states in the HH model,[25–27,29] the present work attempts to directly treat these ordered phases at nonzero temperatures with DMFT + CT-QMC. For SC, we focus on the transition temperature, the superconducting order parameter, and the gap in the one-particle spectral function. We show that the phonon-induced retardation (when the phonon energy is well below the antiadiabatic limit) or the Coulomb repulsion has the effect of significantly decreasing and shifting the T_c dome against $U_{\rm eff}$, and a similar shift occurs for the superconducting order parameter as well. In order to understand and interpret the observed behavior we use an effective static model in a polaron representation with reduced bandwidth derived from a Lang-Firsov transformation, which has been introduced to investigate electron-phonon coupled systems in the strong-coupling or antiadiabatic regime.[34–36] We test the quantitative and qualitative reliability of the effective model by examining to what extent the model reproduces the transition temperature, superconducting order parameter, and Green's function. We also reveal the behavior of the gap and show that the retardation and the Coulomb interaction increase the deviation from BCS theory. As for AF and CO phases, we determine the phase diagram around $U_{\rm eff} = 0$ at nonzero temperature and show how these phases compete with each other.

This paper is organized as follows. In Sec. II, we introduce the Holstein-Hubbard model and explain how DMFT can deal with ordered phases of this model. We also derive the effective static model. In Sec. III, we discuss how the properties of the superconducting state depend on the parameters U, λ, and ω_0 when these parameters are comparable to the bandwidth. We also show phase diagrams at nonzero temperatures around $U = \lambda$ and reveal how AF and CO compete with each other. Section IV gives a brief summary.

II. FORMALISM

A. Model

The HH model represents an electron system that is coupled to local (Einstein) phonons. The Hamiltonian is

$$H = -t \sum_{\langle i,j\rangle,\sigma} [c^\dagger_{j\sigma} c_{i\sigma} + \text{H.c.}] + \sum_i [U n_{i\uparrow} n_{i\downarrow} - \mu(n_{i\uparrow} + n_{i\downarrow})] + g \sum_i (b^\dagger_i + b_i)(n_{i\uparrow} + n_{i\downarrow} - 1) + \omega_0 \sum_i b^\dagger_i b_i, \quad (1)$$

where i, j denote sites, σ is the spin, and the first sum is over nearest neighbors. $c^\dagger_{i,\sigma}$ denotes a creation operator of an electron, $b^\dagger_i$ is a creation operator of a phonon, t is the hopping parameter, U is the on-site electron-electron interaction, μ is the chemical potential, g is the coupling constant between electrons and phonons, and ω_0 is the phonon frequency. In this model, the phonon is envisaged as an optical mode with an approximately constant energy dispersion (Einstein model). Since the phonons are assumed to be noninteracting, one can integrate out the phonon part to derive the effective electron-electron interaction,

$$U_{\rm eff}(\omega) = U - \frac{2g^2\omega_0}{\omega_0^2 - \omega^2}, \quad (2)$$

in a path integral framework. The effective interaction in the low-energy regime is thus

$$U_{\rm eff} \equiv U_{\rm eff}(\omega = 0) \equiv U - \lambda, \quad \lambda = 2g^2/\omega_0. \quad (3)$$

If we take the antiadiabatic limit of $\omega_0 \to \infty$ with λ and U fixed, the HH model reduces to the Hubbard model with the interaction $U_{\rm eff}$. This low-energy effective interaction has been used as a measure of the characteristic effective net interaction in previous works.[10,26,27] In the present work we examine the validity of a static description in the parameter regime of interest, namely, strong electron-electron and electron-phonon coupling, with phonon frequencies comparable to the bandwidth. We shall see that a proper static description involves the screened interaction, along with a reduced bandwidth.

In order to deal with SC states, we employ the Nambu formalism and define the local Green's function as

$$\hat{G}_{{\rm loc},i}(\tau) \equiv -\langle T \Psi_i(\tau) \Psi^\dagger_i(0) \rangle_H = \begin{bmatrix} G_{11,i}(\tau) & G_{12,i}(\tau) \\ G_{21,i}(\tau) & G_{22,i}(\tau) \end{bmatrix}, \quad (4)$$

where $\Psi^\dagger_i \equiv (c^\dagger_{i\uparrow}, c_{i\downarrow})$ are Nambu spinors. We use

$$\Phi = \langle c_{i\downarrow} c_{i\uparrow} \rangle_H = G_{12}(\tau = 0^+) \quad (5)$$

as the order parameter for the SC phase (assuming homogeneity), where $\langle\rangle_H$ denotes the equilibrium expectation value computed with the Hamiltonian H.

B. Dynamical mean-field theory

DMFT, which is exact in infinite spatial dimensions,[18–20] maps a lattice problem onto an effective impurity problem. When we take into account the superconducting state of the

Holstein-Hubbard model, the Hamiltonian of the impurity problem is $H_{\rm imp} = H_{\rm loc} + H_{\rm bath} + H_{\rm mix}$, with the three terms

$$H_{\rm loc} = U n_\uparrow n_\downarrow - \mu(n_\uparrow + n_\downarrow) + g(b^\dagger + b)(n_\uparrow + n_\downarrow - 1) + \omega_0 b^\dagger b, \quad (6)$$

$$H_{\rm bath} = \sum_{\sigma,p} \epsilon_p c^\dagger_{p\sigma} c_{p\sigma} + \sum_p (\Delta_p c^\dagger_{p\uparrow} c^\dagger_{-p\downarrow} + \text{H.c.}), \quad (7)$$

$$H_{\rm mix} = \sum_{\sigma,p} \left(V^\sigma_p d^\dagger_\sigma c_{p\sigma} + \text{H.c.}\right). \quad (8)$$

Here, d is the annihilation operator of the electron on the impurity, n_σ is the density of electrons with spin σ on the impurity, b is the annihilation operator of a local phonon coupled to the impurity, and $c_{p\sigma}$ is the annihilation operator of a spin-σ electron in the bath with the bath states labeled by the quantum number p. In a SC state the parameters Δ_p can be nonzero. Thus the Hamiltonian describes an impurity that is coupled to local phonons in a superconducting bath. The bath ($H_{\rm bath}$) and mixing ($H_{\rm mix}$) terms are determined self-consistently in such a way that the impurity Green's function reproduces the local lattice Green's function of the HH model. The only information on the lattice structure that enters a DMFT calculation is the density of states. Here we adopt the Bethe lattice, a bipartite lattice whose density of states is $\rho(\epsilon) = \frac{1}{\pi t}\sqrt{1 - [\epsilon/(2t)]^2}$.

Since we want to describe phases such as the AF and CO ones with a broken Z_2 symmetry between sublattices, we introduce sublattice indices $\theta = A, B$ ($\bar\theta = B, A$) and express the self-consistency equation in the form

$$[\hat\Lambda_\theta]_{i,j}(\tau) = -\langle T A_i(\tau) A^\dagger_j(0)\rangle_{H_{\rm bath}} = [t^2 \sigma_3 \hat G_{{\rm loc},\bar\theta}(\tau)\sigma_3]_{i,j}, \quad (9)$$

where $\hat\Lambda$ is the hybridization function of the impurity model. Here, $A_i = \sum_p V^i_p a_{p,i}$, $V^1_p = V^\uparrow_p$, $V^2_p = -V^\downarrow_p$, $(a^\dagger_{p,1}, a^\dagger_{p,2}) \equiv (c^\dagger_{p,\uparrow}, c_{-p,\downarrow})$ (all quantities for sublattice θ), and $\sigma_3 = {\rm diag}(1,-1)$ is a Pauli matrix. If we assume a homogenous system, as in the investigation of SC, then $\hat\Lambda_\theta(\tau) = \hat\Lambda(\tau)$ is independent of the sublattice.

The impurity problem, Eqs. (6)–(8), is solved with the continuous-time quantum Monte Carlo impurity solver [hybridization expansion, i.e., we regard the mixing term (8) as a perturbation term and perform a Monte Carlo sampling of the corresponding diagrammatic expansion][37,38] based on the method introduced in Ref. 21. In this approach, a Lang-Firsov decoupling[39] of the electrons and phonons and an analytical summation of all phonon contributions for each term in the expansion enables an exact treatment of the quantum phonons. In the present case, we extend this technique to impurity problems that couple to a superconducting bath.[40] From the methodological point of view, an interesting observation is that the simulations in the SC phase yield more accurate Green's functions than corresponding calculations in the AF phase. This suggests that the sampling and measurement involving off-diagonal hybridization functions produces significantly better statistics and allows us to reliably measure the small values of insulating Green's functions near $\tau = \beta/2$. We discuss this issue in more detail in Appendix A.

C. Effective static model

Before presenting the DMFT results, let us first introduce an effective static model for the low-energy description of the HH model,[34,36] which is useful for discussing the properties of the SC phase. The first step in the derivation is to perform a Lang-Firsov (LF) canonical transformation of the HH model, $H_{\rm LF} = e^S H e^{-S}$, with $S = \frac{g}{\omega_0}\sum_i (n_i - 1)(b^\dagger_i - b_i)$. The explicit expression for $H_{\rm LF}$ is

$$H_{\rm LF} = -t \sum_{\langle i,j\rangle,\sigma} \left[e^{\frac{g}{\omega_0}(b^\dagger_i - b_i)} e^{-\frac{g}{\omega_0}(b^\dagger_j - b_j)} c^\dagger_{i,\sigma} c_{j,\sigma} + \text{H.c.}\right] + U_{\rm eff}\sum_i n_{i,\uparrow} n_{i,\downarrow} - \mu_{\rm eff}\sum_i n_i + \omega_0 \sum_i b^\dagger_i b_i, \quad (10)$$

with $\mu_{\rm eff} = \mu - g^2/\omega_0$. Here, $c^\dagger$, after the LF transformation, has the meaning of creating a polaron, as is evident from the phonon factors. An effective low-energy model for the original fermions is obtained by assuming that the phonons are not much excited. In other words, the effective Hamiltonian for the fermion part is obtained as the projection onto the subspace of zero phonons, $H_{\rm eff} = \langle 0|H_{\rm LF}|0\rangle$, where $|0\rangle$ is the phonon vacuum state. This description becomes exact in the limit where ω_0 is large and the temperature is much lower than ω_0. The Hamiltonian resulting from the projection is[34]

$$H_{\rm eff} = -Z_B t \sum_{\langle i,j\rangle,\sigma} [c^\dagger_{i,\sigma} c_{j,\sigma} + \text{H.c.}] + U_{\rm eff}\sum_i n_{i,\uparrow} n_{i,\downarrow} - \mu_{\rm eff}\sum_i n_i,$$
$$Z_B = \exp\left(-g^2/\omega_0^2\right). \quad (11)$$

This is nothing but the usual Hubbard model with a static interaction $U_{\rm eff}$ and a hopping parameter renormalized by Z_B. From this model we can readily derive physical quantities such as the transition temperature, the order parameter for the SC phase, or the Green's functions from simulations of the Hubbard model as follows: Let us define $\Phi(T, U, U_{\rm eff}, Z_{\rm B}) = \langle c_\downarrow c_\uparrow\rangle_H$ as the order parameter for the SC state. Within the effective model, the order parameter is expressed as

$$\begin{aligned}\Phi(T,U,U_{\rm eff},Z_{\rm B}) &= \langle e^{-2\frac{g}{\omega_0}(b^\dagger - b)} c_\downarrow c_\uparrow\rangle_{H_{\rm LF}} \\ &\approx \langle 0|e^{-2\frac{g}{\omega_0}(b^\dagger - b)}|0\rangle \langle c_\downarrow c_\uparrow\rangle_{H_{\rm eff}} \\ &= Z_B^2 \Phi_0(T/Z_B, U_{\rm eff}/Z_B) \\ &\equiv \Phi_{\rm eff}[T, Z_B, U_{\rm eff}], \end{aligned} \quad (12)$$

where we have defined $\Phi_0(T,U)$ as the order parameter for the Hubbard model with hopping t and interaction U at temperature T. It follows that the transition temperature for the Holstein-Hubbard model ($T_c[U, U_{\rm eff}, Z_B]$) is related to that for the attractive Hubbard model ($T_c^0[U]$) by

$$\begin{aligned} T_c[U, U_{\rm eff}, Z_{\rm B}] &\approx Z_{\rm B} T_c^0[U_{\rm eff}/Z_{\rm B}] \\ &\equiv T_{c,\rm eff}[Z_B, U_{\rm eff}]. \end{aligned} \quad (13)$$

In order to evaluate Green's functions, we again use the LF transformation to obtain

$$G_\sigma(\tau) = -\langle T_\tau c_\sigma(\tau) c_\sigma^\dagger(0)\rangle_H = -\left\langle T_\tau e^{-\frac{g}{\omega_0}[b^\dagger(\tau)-b(\tau)]} c_\sigma(\tau) e^{\frac{g}{\omega_0}[b^\dagger(0)-b(0)]} c_\sigma^\dagger(0)\right\rangle_{H_{\rm LF}}. \quad (14)$$

Then we make an approximation and separate the phonon factors from the expectation value with respect to $H_{\rm LF}$ (i.e., the phonon dynamics may be decoupled from the polaron dynamics for large enough ω_0). The fermionic part is evaluated by the static approximation, which gives

$$G_\sigma(\tau) \approx -\langle T_\tau c_\sigma(\tau) c_\sigma^\dagger(0)\rangle_{H_{\rm eff}} \times \left\langle T_\tau e^{-\frac{g}{\omega_0}[b^\dagger(\tau)-b(\tau)]} e^{\frac{g}{\omega_0}[b^\dagger(0)-b(0)]}\right\rangle_{H_{\rm ph}}, \quad (15)$$

where $H_{\rm ph} = \omega_0 \sum_i b_i^\dagger b_i$. In other words, we treat the whole system as if its Hamiltonian is $H_{\rm eff} + H_{\rm ph}$.[35]

As for the anomalous part, we have

$$G_{12}(\tau) \approx -\langle T_\tau c_\uparrow(\tau) c_\downarrow(0)\rangle_{H_{\rm eff}} \times \left\langle T_\tau e^{-\frac{g}{\omega_0}[b^\dagger(\tau)-b(\tau)]} e^{-\frac{g}{\omega_0}[b^\dagger(0)-b(0)]}\right\rangle_{H_{\rm ph}}. \quad (16)$$

The phonon factor can be calculated analytically as

$$\left\langle T_\tau e^{-s\frac{g}{\omega_0}[b^\dagger(\tau)-b(\tau)]} e^{-s'\frac{g}{\omega_0}[b^\dagger(0)-b(0)]}\right\rangle_{H_{\rm ph}} = \exp\left\{-\frac{g^2/\omega_0^2}{e^{\beta\omega_0}-1}[(e^{\omega_0\beta}+1) + ss'(e^{\omega_0(\beta-\tau)} + e^{\omega_0\tau})]\right\}, \quad (17)$$

where $s, s' = \pm 1$ and $0 \leqslant \tau \leqslant \beta$.

III. RESULTS

In the following, we use the quarter of the bandwidth, $t = W/4$, as the unit of energy and focus on the case of half filling. Transition temperatures are evaluated from the order parameter in ordered phases.

A. Superconductivity

Here, we investigate the SC phase at half filling in order to understand the effect of the retardation and the Coulomb repulsion on the SC state. To focus on SC, we enforce the symmetries $G_{11}(\tau) = G_{11}(\beta-\tau) = G_{22}(\tau) = G_{22}(\beta-\tau)$, which hold in the SC and normal states at half filling but not in the AF and CO phases. Strictly speaking, if we allow both CO and SC orders in the self-consistency loop, CO dominates over SC. Still, it should be meaningful to study the SC state at half filling since, if the system has a frustration (e.g., induced by a second-neighbor hopping on a bipartite lattice), CO and AF may be suppressed. The results of this section can be thought of as describing the properties of such frustrated systems.

We first show that the Coulomb interaction induces a characteristic structure in the anomalous Green's function. Figure 1(a) plots normal and anomalous Green's functions on the imaginary-time axis. While the diagonal Green's functions are negative and symmetric (at half filling), the off-diagonal Green's functions are antisymmetric around $\tau/\beta = 0.5$. In

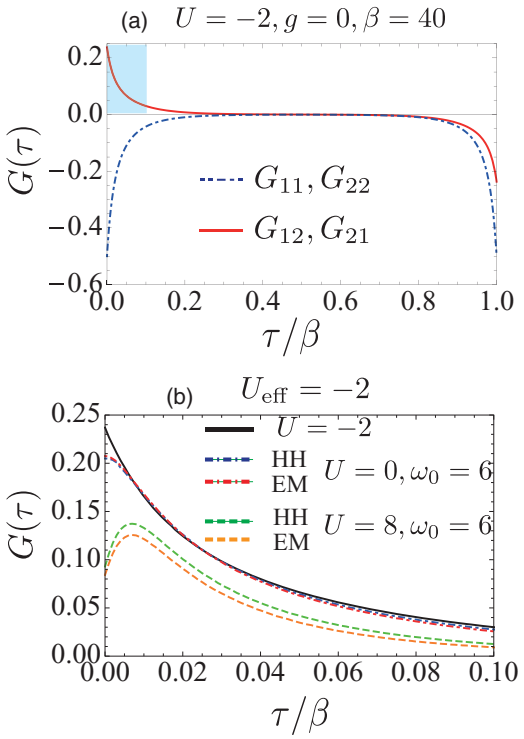

FIG. 1. (Color online) (a) Typical behavior of Green's functions on the imaginary-time axis, here for $U=-2$, $g=0$, and $\beta=40$. (b) A close-up [blue region in (a)] of the anomalous Green's function for various g and U and fixed $U_{\rm eff}=-2$ ($\omega_0=6$ and $\beta=40$). HH means the Green's function is computed from the HH model, while EM means that it is obtained with the effective model.

Fig. 1(b) we show the short-time behavior of the anomalous Green's functions for different sets of parameter values: without retardation (Hubbard model with $U=-2$), with only a retarded attractive interaction ($U=0$ and $\omega_0>0$), and with both retardation and Coulomb repulsion. In all three cases, $U_{\rm eff}=-2$, $\omega_0=6$, and $T=0.025$. Without the retardation, the anomalous Green's function has its maximum at $\tau=0$. In the presence of a retarded attractive interaction but without U, the position of the maximum remains at $\tau=0$, but the peak is rounded off. If we then switch on a $U>0$, the peak shifts to $\tau>0$, which indicates that when electrons form pairs, they tend to avoid the instantaneous repulsive interaction U while exploiting the retarded attractive interaction.

One can explain the origin of this behavior with the effective model, Eq. (16). The corresponding results are also shown in Fig. 1(b). It turns out that the shift of the peak with U in the anomalous Green's function is well reproduced by the effective model. This structure comes from the phonon part, Eq. (17), which increases with τ near $\tau=0$ and becomes steeper with U for a fixed $U_{\rm eff}$.

Next, we clarify the effect of the two different interactions on the phase diagram. In Fig. 2 we plot T_c as a function of $-U_{\rm eff}$. For all the parameter sets one can find that T_c rises with $-U_{\rm eff}$ in the weak-coupling regime while it decreases in the strong-coupling regime. This forms a T_c dome, indicating a BCS-BEC crossover. The strong-coupling regime is characterized by the condensation of bipolarons, which

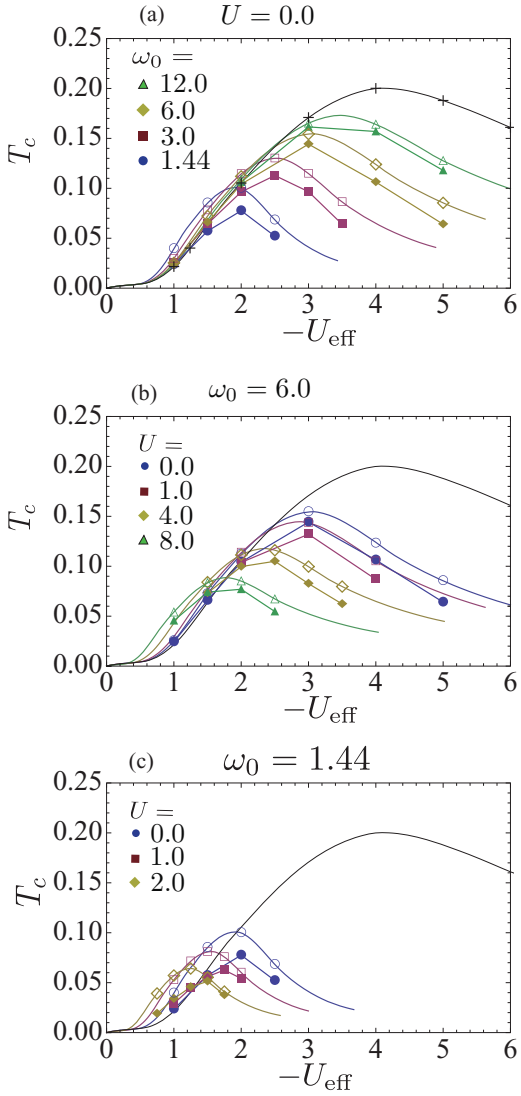

FIG. 2. (Color online) T_c against $-U_{\rm eff}$ for various sets of parameter values. Solid markers are DMFT + QMC results. (a) shows the dependence on ω_0 for $U = 0$. The lines connecting symbols are guides for the eye. (b) and (c) show the phase diagram when U is switched on with a fixed value of (b) $\omega_0 = 6$ or (c) $\omega_0 = 1.44$. The crosses in (a) show the results for the attractive Hubbard model with $-U_{\rm eff}$, and the black curve in each panel indicates the corresponding T_c. The colored curves show the results from the effective model, and open markers on these lines should be compared with the solid markers with the same shape.

are electron pairs bound by the phonon-mediated attractive retarded interaction.

Let us discuss the dependence of T_c on the retardation and the Coulomb interaction in detail. Figure 2(a) illustrates the effect of the retardation (controlled by ω_0) on the SC phase for the case $U = 0$. As ω_0 decreases, the position of the peak in T_c shifts to the weak-$|U_{\rm eff}|$ regime, while the height of the peak decreases. We also note that the T_c in the weak-coupling regime still agrees well with that of the attractive Hubbard model with interaction $U_{\rm eff}$. This result should be contrasted with the behavior of CO in the Holstein model.[41,42] The shift of the T_c dome with ω_0 is also observed in the CO case, while the height of the T_c peak does not show a significant change. Furthermore, in the case of CO, the transition temperature increases in the weak-coupling regime when $U_{\rm eff}$ is fixed and ω_0 decreases.[41,42] The difference between SC and CO in the weak-coupling region can be explained as follows: The important interaction for SC is the interaction between electrons with opposite spins. For CO, however, the phonon-mediated interaction between electrons with the same spin is also relevant, as can be understood from a mean-field analysis in the adiabatic limit (see Appendix B). When the phonon frequency is reduced, the lattice distortion takes so much time that an electron starts to feel the attraction from another electron with the same spin through this distortion. Due to this additional attraction, T_c increases in the CO case, when ω_0 decreases, while SC cannot take advantage of it.

In Figs. 2(b) and 2(c), the effect of the Coulomb repulsion is illustrated. As U increases, the position of the peak shifts to the weak-coupling regime, and the height of the peak decreases. It turns out that the T_c in the weak-coupling region is not necessarily well reproduced by the attractive Hubbard model with interaction strength $U_{\rm eff}$ [see, e.g., $U = 8$ in Fig. 2(b) or $U = 2$ in Fig. 2(c)]. Here we note that the investigation of larger $U_{\rm eff}$ is difficult since our sampling processes are not so efficient in this regime. One possible solution is to add special Monte Carlo updates suggested in Ref. 43, but we have not implemented them.

Let us now examine the above properties in terms of the low-energy effective static model in the polaron representation, which is a Hubbard model with interaction $U_{\rm eff}$ *and* a renormalized hopping parameter [reduced by the factor Z_B; see Eq. (11)]. The resulting transition temperature provides a qualitatively good description of the dependence of the transition temperature on ω_0, U, and λ (see colored curves in Fig. 2). The effective model always somewhat overestimates the transition temperature. An increase in U or a decrease in ω_0 with $U_{\rm eff}$ fixed leads to an increase of $Z_B = \exp(-\frac{\lambda}{2\omega_0})$ since $\lambda = U - U_{\rm eff}$. Therefore the band renormalization for the polaron enhances the effect of interactions between polarons, which may be characterized by the ratio between $U_{\rm eff}$ and the bare-polaron band width $Z_B W$, where $W = 4t$ is the band width of bare electrons. As a result, the peak of the transition temperature shifts to smaller $|U_{\rm eff}|$. Note that the effective model also shows that, with larger U, the deviations from the attractive Hubbard model (black lines in Fig. 2) increase in the weak-coupling regime [see, for example, the colored lines for $U = 8$ in Fig. 2(b) or $U = 2$ in Fig. 2(c)]. This is related to the fact that the shape of T_c in the attractive Hubbard model is convex in the weak-coupling (BCS) regime. Therefore the enhancement of the correlations due to the renormalization of the hopping parameter by Z_B can lead to deviations from the attractive Hubbard model if we do not rescale the $U_{\rm eff}$ axis. Here one may wonder why, when ω_0 is changed with $U = 0$ and $U_{\rm eff}$ is fixed, the deviation from the attractive Hubbard model is not as apparent as it is when U is changed with ω_0 and $U_{\rm eff}$ is fixed. This is because we need smaller ω_0 to realize a given value of Z_B when $U = 0$, while the reliability of the effective model is degraded for smaller ω_0. Related to this, let us also comment on the relation between the present work and conventional analyses or extensions thereof. Here we have shown that the effective model provides a good

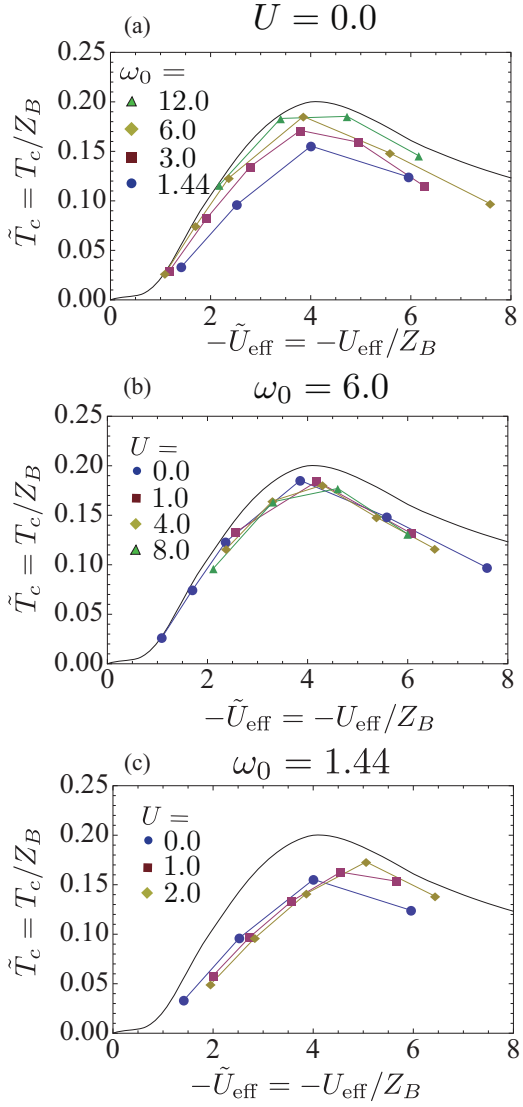

FIG. 3. (Color online) The phase diagram with rescaled parameters: $\tilde{U}_{\rm eff} \equiv U_{\rm eff}/Z_B$ and $\tilde{T}_c \equiv T_c/Z_B$. (a) shows the result for various values of ω_0 at $U = 0$. (b) and (c) show the result when U is switched on with a fixed (b) $\omega_0 = 6$ or (c) $\omega_0 = 1.44$. The black curve in each panel shows T_c in the attractive Hubbard model with $-\tilde{U}_{\rm eff}$.

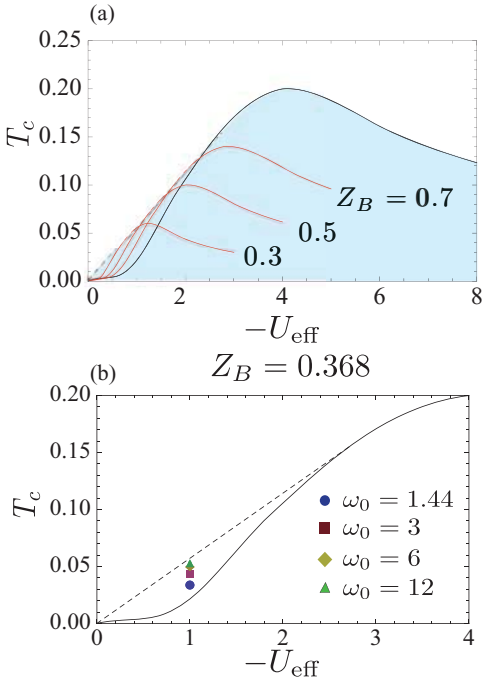

FIG. 4. (Color online) (a) Possible area (shaded) for the SC phase in the Holstein-Hubbard model, defined by the envelope of the T_c curves (red) for various values of Z_B. The black solid curve represents the behavior in the attractive Hubbard model with $-U_{\rm eff}$, while the dashed line shows the envelope of the curves when Z_B is varied. (b) T_c vs $-U_{\rm eff}$ for various values of ω_0, plotted here for $U_{\rm eff} = -1$, $Z_B = U_{\rm eff}/U_0$.

description of the effect of the retardation and the effect of the Coulomb interaction when ω_0 is comparable to or larger than the bandwidth of the bare electrons W. On the other hand, when ω_0 is much smaller than W, the present picture becomes inadequate. Instead, the Migdal theorem becomes applicable for the phonons,[30] and a description in terms of μ^*, which is the reduced Coulomb interaction due to the retardation effect, works well.[29,32,33] A recent extension of these conventional theories has revealed that the μ^* picture works well even up to the intermediate-coupling regime.[29]

If the effective model reproduces the Holstein-Hubbard model results perfectly, the phase diagram in the space of $\tilde{T}_c \equiv T_c/Z_B$ and $\tilde{U}_{\rm eff} \equiv U_{\rm eff}/Z_B$ should coincide with that of the attractive Hubbard model. Our numerical data, replotted in terms of $\tilde{U}_{\rm eff}$ and $\tilde{T}$ in Fig. 3, cover the range $2 \lesssim |\tilde{U}_{\rm eff}| \lesssim 6$. As expected, the reliability of the effective model becomes better as ω_0 increases [Fig. 3(a)]. For $U = 0$, the relative deviation [$\delta T_c \equiv |T_c - T_{c,\rm eff}|/T_c$, where $T_{c,\rm eff}$ is defined in Eq. (13)] is smallest at intermediate coupling ($|\tilde{U}_{\rm eff}| \sim 4$) for each ω_0. The deviation decreases from $\delta T_c \leqslant 0.25$ for $\omega_0 = 4$ to $\delta T_c \leqslant 0.1$ for $\omega_0 = 12$. The dependence of δT_c on $U_{\rm eff}$ is relatively small at $\omega_0 \geqslant 4$. On the other hand, if $\omega_0 \leqslant 2$, the reliability of the effective model strongly depends on $U_{\rm eff}$, as shown in Fig. 3(a). As for the effect of U, we find that δT_c slightly, but systematically, increases with increasing U, at least in the weak-coupling regime [Figs. 3(b) and 3(c)], and at $\omega_0 = 4$, $\delta T_c \leqslant 0.25$ up to $U = 4$. The effective model is quantitatively accurate up to larger values of U for larger ω_0.

The above analysis enables us to discuss the region in the T versus $-U_{\rm eff}$ space, where a superconducting phase of the Holstein-Hubbard model can exist. The shaded area in Fig. 4(a) shows this region as predicted by the effective model. The boundary of this area is defined by the various T_c curves with different Z_B. It rises from the origin linearly and touches the T_c curve of the attractive model before the peak. This is because the T_c curves for various values of Z_B form a homologous series of phase boundaries of the attractive Hubbard model, Eq. (13). In the weak-coupling regime of the Hubbard model, the phase boundary is convex, while the boundary is concave in the intermediate-coupling regime, where the BCS-BEC crossover occurs. The envelope indeed becomes a tangent to the original curve (black solid curve in Fig. 4) at $U_{\rm eff} \simeq -2.72 \equiv U_0$. The boundary of the blue area is obtained by fixing $U_{\rm eff}$, $Z_B = U_{\rm eff}/U_0$ and taking

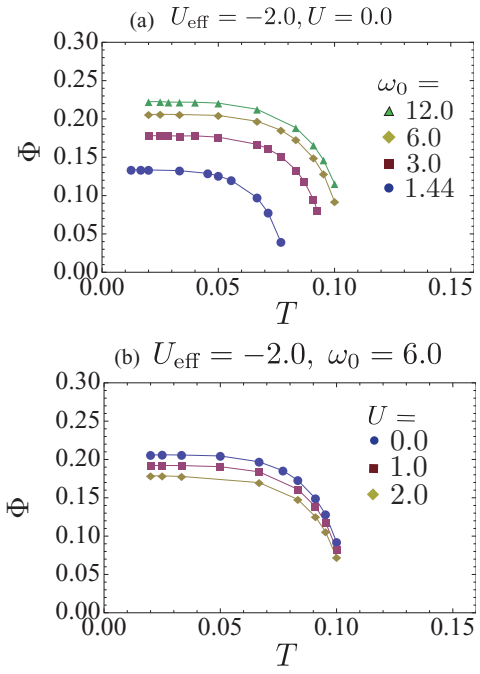

FIG. 5. (Color online) Temperature dependence of the superconducting order parameter $\Phi(T)$ (a) for $U_{\rm eff} = -2, U = 0$ and various values of ω_0 and (b) for $U_{\rm eff} = -2, \omega_0 = 6$ and various values of U.

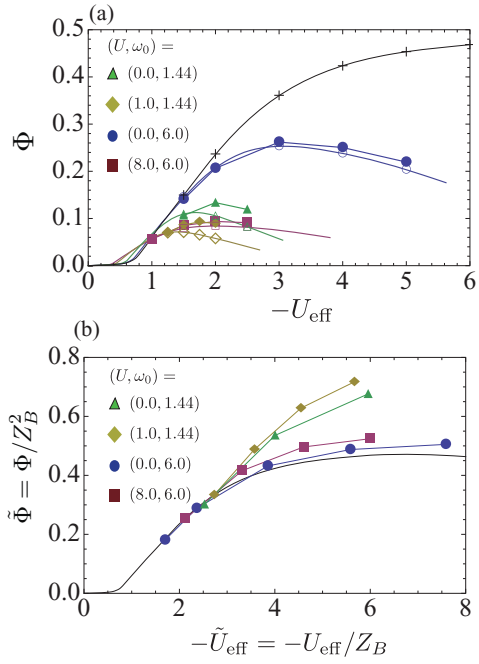

FIG. 6. (Color online) The superconducting order parameter in the limit of $T \to 0$ [$\Phi(T \to 0)$]. Solid markers are DMFT + QMC results. (a) plots the result against $-U_{\rm eff}$ for various sets of parameter values. The crosses are $\Phi(T \to 0)$ for the attractive Hubbard model, and the black curve is an interpolation. The colored curves show the results from the effective model, and open markers on these lines should be compared with the solid markers with the same shape. (b) plots the results on rescaled axes: $\tilde{U}_{\rm eff} \equiv U_{\rm eff}/Z_B$ and $\tilde{\Phi} \equiv \Phi/Z_B^2$.

the limit $\omega_0 \to \infty$ (see Fig. 4). The effective model always overestimates the transition temperature in the parameter region studied here, so that we expect that the superconducting phase of the Holstein-Hubbard model is contained within the blue area. We note that when we take the limit $\omega_0 \to \infty$ with $U_{\rm eff}$, Z_B fixed, $U_{\rm eff}(\omega) \to U_{\rm eff}$ for every finite ω, but because $\lambda \to \infty$, this does not mean that the Holstein-Hubbard model becomes the attractive Hubbard model without bandwidth reduction.

Next, we discuss the properties of the superconducting state itself. We first consider the temperature dependence of the superconducting order parameter $\Phi(T)$. In Fig. 5(a) we fix $U = 0$, $U_{\rm eff} = -2$ and change the value of ω_0. In Fig. 5(b) we fix $\omega_0 = 6$, $U_{\rm eff} = -2$ and change U. Φ monotonically increases below T_c and saturates as the temperature is decreased. As can be seen in Figs. 5(a) and 5(b), the retardation and the Coulomb repulsion U both act to decrease $\Phi(T)$.

In order to investigate the effect of the two types of interactions on the superconducting order parameter more systematically, we focus on the value of Φ in the limit of $T \to 0$ (Fig. 6). In Fig. 6(a), $\Phi(T \to 0)$ is plotted as a function of $-U_{\rm eff}$. In the attractive Hubbard model, $\Phi(T \to 0)$ saturates at 0.5 in the strong-coupling limit.[43] On the other hand, for finite ω_0, we find that it has a peak as a function of $-U_{\rm eff}$. Furthermore, the peak shifts to smaller $|U_{\rm eff}|$ as the retardation increases (ω_0 decreases) or the Coulomb interaction U increases. We also note that, in the region investigated ($-U_{\rm eff} \gtrsim 1.5$), $\Phi(T \to 0)$ decreases as ω_0 decreases or U increases, as illustrated in Fig. 5. It turns out that this behavior is qualitatively well described by the effective model, as shown by the colored lines in Fig. 6(a).

One can understand the origin of the peak structure in $\Phi(T \to 0)$ as follows: Within the effective model, what saturates at large $U_{\rm eff}$ for $\omega_0 \neq 0$ is the density of pairs of polarons, which can be expressed as $\langle c_\downarrow c_\uparrow \rangle_{\rm LF}$ after the Lang-Firsov transformation, while Φ, the order parameter defined for electrons, has some correction coming from the phonon dressing. This correction becomes large as the electron-phonon coupling becomes large; see Eq. (12) (Z_B decreases as λ increases). Related to the discussion of Fig. 5, we also have to note that the effective model, in the weak-coupling region, predicts that there is some area where $\Phi(T \to 0)$ increases as ω_0 decreases or U increases. However, within our approach (CT-QMC based on the hybridization expansion), this region is difficult to access since it is in the weak-coupling regime and at very low temperature.

In order to assess the potential of the effective model to reproduce the superconducting order parameter, we rescale the axis of Fig. 6(a) as $\tilde{U}_{\rm eff} \equiv U_{\rm eff}/Z_B$ and $\tilde{\Phi} \equiv \Phi/Z_B^2$ and show the result in Fig. 6(b). Again we focus on the range $2 \lesssim |\tilde{U}_{\rm eff}| \lesssim 6$. It turns out that, with large enough $|\tilde{U}_{\rm eff}|$, the rescaled curve underestimates $\Phi(T \to 0)$, while for smaller $|\tilde{U}_{\rm eff}|$ ($\lesssim 2.5$), the effective model becomes better. A larger U leads to a larger underestimation in the strong $|\tilde{U}_{\rm eff}|$ regime. Quantitatively, $\delta\Phi \equiv |[\Phi(T \to 0) - \Phi_{\rm eff}(T \to 0)]|/\Phi(T \to 0) \leqslant 0.2$ for $\omega_0 \gtrsim 4$ at $U = 0$, where $\Phi_{\rm eff}$ is defined in Eq. (12). As for the effect of U, we find $\delta\Phi \leqslant 0.2$ up to $U = 6$ at $\omega_0 = 4$. The effective model is quantitatively accurate up to larger U for larger ω_0. The reliability of the effective model for Φ is slightly better than in the case of the transition temperature.

Now let us move on to discuss the energy gap in the spectral function and its relation with the transition temperature. We express the self-energy, which is independent of momentum in DMFT, as

$$\hat{\Sigma}(i\omega_n) = \begin{bmatrix} \Sigma(i\omega_n) & S(i\omega_n) \\ S(i\omega_n) & -\Sigma^*(i\omega_n) \end{bmatrix}, \tag{18}$$

where Σ is the normal self-energy, while S is the anomalous one. Then the lattice Green's function in momentum space is

$$\begin{aligned} \hat{G}(\mathbf{k},i\omega_n) &= \begin{bmatrix} G_{11}(\mathbf{k},i\omega_n) & G_{12}(\mathbf{k},i\omega_n) \\ G_{21}(\mathbf{k},i\omega_n) & G_{22}(\mathbf{k},i\omega_n) \end{bmatrix} \\ &= [|G^0(\mathbf{k},i\omega_n)^{-1} - \Sigma(i\omega_n)|^2 + |S(i\omega_n)|^2]^{-1} \begin{bmatrix} G^0(-\mathbf{k},-i\omega_n)^{-1} - \Sigma(-i\omega_n) & -S(i\omega_n) \\ -S(i\omega_n) & -G^0(\mathbf{k},i\omega_n)^{-1} + \Sigma(i\omega_n) \end{bmatrix}, \end{aligned} \tag{19}$$

where $G^0(\mathbf{k},i\omega_n) = i\omega_n - (\epsilon_\mathbf{k} - \mu)$ is the bare lattice Green's function and $\epsilon_\mathbf{k}$ is the dispersion relation for the bare electrons. If we make an analytic continuation ($i\omega_n \to \omega + i0^+$) to obtain the self-energy on the real-frequency axis, the spectral gap in the single-particle spectrum is given by $zS(\omega = 0)$ if the contribution to the self-energy from the terms higher order in ω than $O(\omega)$ is neglected. Here $z \equiv (1 - \partial\Sigma(\omega)/\partial\omega|_{\omega=0})^{-1}$ is the quasiparticle weight.

With Dyson's equation and Eq. (9), one finds for the Bethe lattice that

$$\hat{\Sigma}(i\omega_n) = i\omega_n\sigma_0 + \mu\sigma_3 - t^2\sigma_3\hat{G}_{\rm loc}(i\omega_n)\sigma_3 - \hat{G}^{-1}_{\rm loc}(i\omega_n), \tag{20}$$

where σ_0 is the identity matrix. If the quasiparticle picture is good, we can express the self-energies for small $|\omega_n|$ as

$$\Sigma(i\omega_n) = \Sigma^{(0)} + i\omega_n\Sigma^{(1)} + O((i\omega_n)^2), \tag{21}$$

$$S(i\omega_n) = S(\omega = 0) + O((i\omega_n)^2), \tag{22}$$

where $\Sigma^{(0)} \equiv \Sigma(\omega = 0)$, $\Sigma^{(1)} \equiv \partial\Sigma(\omega)/\partial\omega|_{\omega=0}$. One can then evaluate z and $S(\omega = 0)$ with the information on the Matsubara axis. If one approximates the quasiparticle weight z by $Z \equiv [1 - {\rm Im}\Sigma(\omega_{n=0})/\omega_{n=0}]^{-1}$ and $S(\omega = 0)$ by $S^{(0)} \equiv [9S(\omega_{n=0}) - S(\omega_{n=1})]/8$, one finds that the gap in the excitation spectrum is

$$\Delta \equiv ZS^{(0)}. \tag{23}$$

This provides a rough estimate of the spectral gap. We have to note that this approximation, which uses the information around $\omega = 0$, is good in the weak-coupling regime and when the gap is small enough. When $U_{\rm eff}$ becomes larger, this analysis becomes worse. However, it turns out that the gap estimated in this way is reasonable even in the strong-coupling regime, judging from the comparison with a previous work for the Hubbard model,[44] although the structure of the spectrum is different. In the BCS theory, the ratio between the energy gap and the transition temperature $[2\Delta(T \to 0)/T_c]$ is 3.528, so that any deviation from this value is a measure for the deviation from the BCS theory.

Figure 7 displays the gap Δ (estimated as described above) in the limit of $T \to 0$. Δ turns out to monotonically increase with $|U_{\rm eff}|$ in all cases. When we decrease ω_0 for a fixed $U = 0$, Δ does not necessarily change monotonically with ω_0 for each value of $U_{\rm eff}$, and the dependence on ω_0 is small [see Fig. 7(a)]. On the other hand, for fixed ω_0 and $|U_{\rm eff}|$, the gap increases with U.

Figure 8 plots $2\Delta(T \to 0)/T_c$. We can notice that this quantity significantly increases, again monotonically, with $|U_{\rm eff}|$. In the opposite limit of $|U_{\rm eff}| \to 0$, $2\Delta/T_c$ approaches the BCS value of 3.528 in all cases. This is not trivial since even if $|U_{\rm eff}|$ is small, λ and U themselves can be large (as in the case of $U = 8$). Therefore, there is no simple reason why the BCS theory can be applied in that situation. Now, let us take a closer look. In Fig. 8(a) for $U = 0$, one finds that $2\Delta/T_c$ grows with $|U_{\rm eff}|$ faster for smaller ω_0. In other words, the region where the conventional theories work decreases when the phonon becomes softer. However, in the small-$|U_{\rm eff}|$ regime, the dependence on ω_0 becomes weak, which reflects the fact that T_c for small $|U_{\rm eff}|$ is approximately given by the attractive Hubbard model result (hence weakly dependent on ω_0; see Fig. 2), while Δ also exhibits a weak dependence on ω_0. For larger $|U_{\rm eff}|$ an ω_0 dependence of $2\Delta/T_c$ results from the behavior of T_c. Figures 8(b) and 8(c) show the effect of the Coulomb interaction U. It turns out that $2\Delta/T_c$ grows faster for larger U, which suggests that, even though both T_c and Δ increase with U in the small $|U_{\rm eff}|$ regime, the latter increases faster. To sum up, the retardation and the Coulomb interaction lead to deviations from the BCS theory, but if $U_{\rm eff}$ is small enough, the gap is consistent with the BCS prediction.

Finally, let us discuss the relevance of the present results for organic superconductors, such as alkali-doped fullerides[2–4] and aromatic superconductors.[5–9] In these molecular solids, the characteristic frequency of intramolecular phonons is reported to be comparable to the electronic bandwidth or the inverse of the density of states at the Fermi level. For example, Ref. 8 estimates that $\omega_{\ln}N(\epsilon_F) \sim 0.89$ for potassium-doped picene, where $\omega_{\ln}$ is the logarithmically averaged phonon frequency and $N(\epsilon_F)$ is the density of states at the Fermi energy. If we identify $\omega_{\rm nl}$ with ω_0 in our model with $N(\epsilon_F) = \frac{1}{\pi t}$, we have $\omega_0 \sim 2.81t$, while Ref. 5 for the same material estimates $0.95t \lesssim \omega_{\ln} \lesssim 1.35t$. In addition, when $\omega_{\ln}$ is compared with the width of the relevant conduction band ($\sim$0.3 eV),[7,8] which in our case is $W = 4t$, we end up with $\omega_0 \simeq 1.69t$ for the organic material. Since we have found here that the effective static model is qualitatively reliable even for $\omega_0 = 1.44t$ ($\sim W/4$), we expect that the static effective model in the polaron picture is useful to analyze the qualitative behavior such as the material's pressure dependence. We

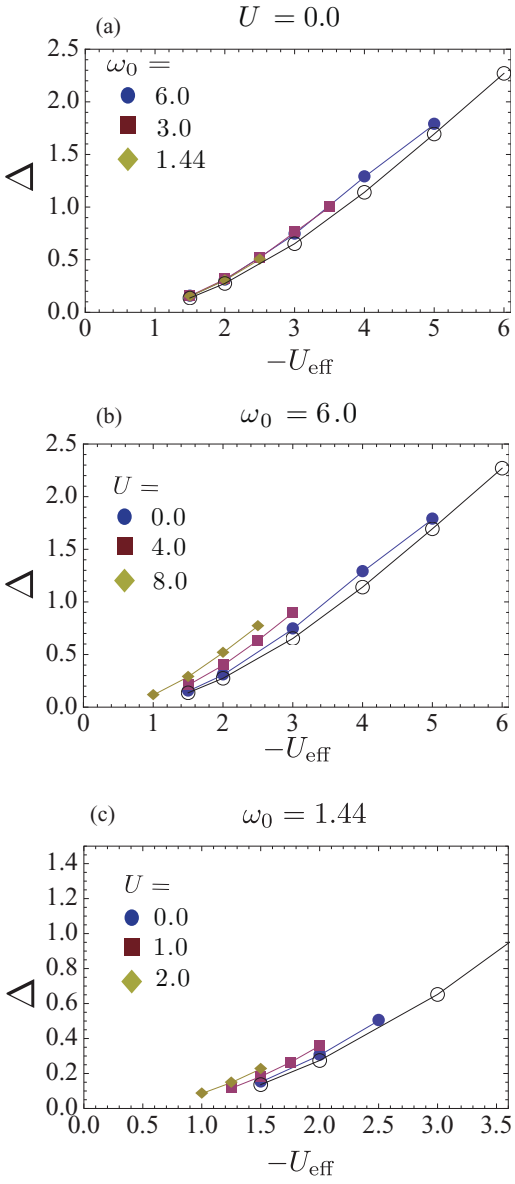

FIG. 7. (Color online) The energy-gap parameter Δ [$= \Delta(T \to 0)$] against $-U_{\rm eff}$ for various sets of parameters. (a) is for various values of ω_0 at $U = 0$ and (b) and (c) are the results when U is switched on with a fixed (b) $\omega_0 = 6$ and (c) $\omega_0 = 1.44$. The open circles are the results for the attractive Hubbard model with $-U_{\rm eff}$ for each panel. Note the different scales of the x and y axes in panel (c) compared to the other panels.

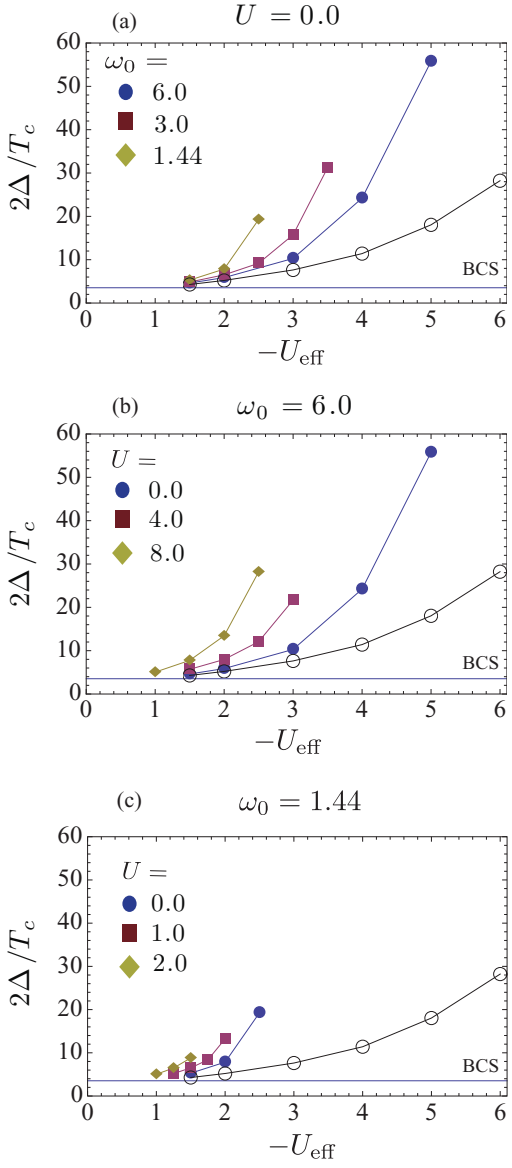

FIG. 8. (Color online) The ratio of the energy-gap parameter to the transition temperature [$2\Delta(T \to 0)/T_c$] against $-U_{\rm eff}$. The horizontal blue line indicates the BCS value $2\Delta/T_c = 3.528$. (a) shows the result for various values of ω_0 at $U = 0$. (b) and (c) are the result with finite U and fixed (b) $\omega_0 = 6$ and (c) $\omega_0 = 1.44$. Open circles show the results for the attractive Hubbard model with $-U_{\rm eff}$.

caution, however, that in a realistic study of organic superconductors, one has to consider multiple molecular orbitals for electrons,[7] with associated multiple types of electron-electron and electron-phonon couplings (Hund's couplings, intraorbital phonon couplings, and/or Jahn-Teller interactions).

B. Antiferromagnetism and charge order

To understand the competition of ordered phases in the presence of two kinds of interactions, we now investigate the Holstein-Hubbard model at nonzero temperatures around $U_{\rm eff} = 0$, without any constraint (i.e., allowing SC, commensurate CO, and commensurate AF). In the following, the order parameter of the CO phase ($\Phi_{\rm CO}$) is defined as $\Phi_{\rm CO} = [(n_{A,\uparrow} + n_{A,\downarrow}) - (n_{B,\uparrow} + n_{B,\downarrow})]/4$, where $n_{A,\sigma}$ ($n_{B,\sigma}$) represents the density of electrons on the A (B) sublattice with spin σ. For the AF phase the order parameter is defined as $\Phi_{\rm AF} = (n_\uparrow - n_\downarrow)/2$, where $n_\uparrow$ ($n_\downarrow$) is the density of up-spin (down-spin) electrons. In the simulations, we use the hybridization functions for $U_{\rm eff} = U - \lambda$ as an input for the next step $U_{\rm eff} = U - \lambda - \delta\lambda$, where $\delta\lambda$ denotes a small increment in λ.

Figure 9 shows the behavior of the order parameters around $U_{\rm eff} = 0$ obtained by varying λ to change $U_{\rm eff}$ for each value of U. Here we fix $\omega_0 = 0.6$ and $\beta = 20$. There is no SC phase, and AF and CO compete with each other. If the interaction U

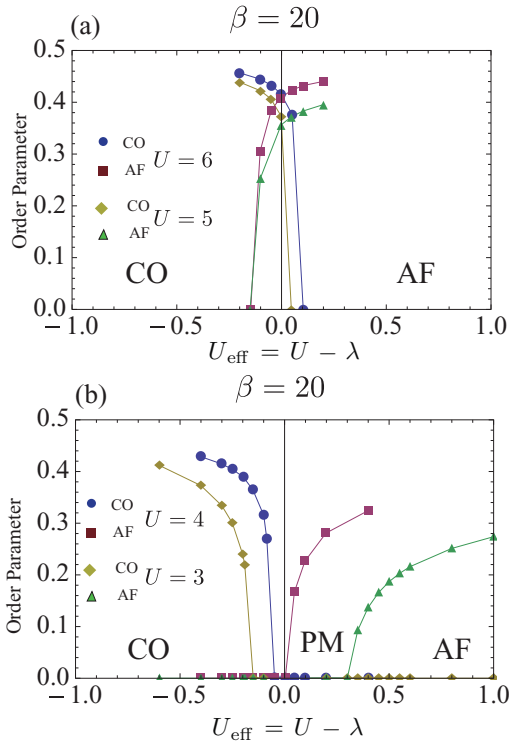

FIG. 9. (Color online) Order parameters against $U_{\rm eff} = U - \lambda$ around $U \sim \lambda$ for a fixed $\omega_0 = 0.6$ at half filling. In (a), the result for $U = 6, 5$ is shown, while (b) shows the result for $U = 4$ and 3 (both at $\beta = 20$). For smaller U, CO and AF are separated by a PM region.

is strong enough [$U = 5, 6$; see Fig. 9(a)], the phase transition is of first order, i.e., the order parameters show a hysteresis around the phase boundary. In other words, there is a region around $U_{\rm eff} = 0$, in which both an AF and a CO solution of the DMFT equations exist. In order to determine the stable solution, one would have to compute the free energies, which is beyond the scope of the present study. On the other hand, if the interaction U is smaller [$U = 3$, 4; see Fig. 9(b)], a paramagnetic metallic phase (PM) appears between the CO and AF phases. This phase has also been found in a QMC analysis of the two-dimensional Holstein-Hubbard model.[17] The transition to PM is second order since the order parameter continuously goes to zero as one approaches the boundary in Fig. 9(b).

We summarize the results by plotting the phase diagrams in the U-λ plane for various conditions in Fig. 10, the phase diagrams in the plane of U and $-U_{\rm eff}$ in Fig. 11, and the phase diagram in the plane of T and $U_{\rm eff}$ (weak-coupling regime) with fixed U and ω_0 in Fig. 12(a).

In the weak-coupling regime, there is a PM around $U_{\rm eff} = 0$ as pointed out above. It turns out that the area of the PM phase is wider on the $U > \lambda$ side than on the opposite side. This can be explained by a mean-field theory in the adiabatic limit, which has been used to explain the first-order transition in the strong-coupling regime at $T = 0$ in Ref. 27. This approximation indicates that the interaction that appears in the gap equation is $U - 2\lambda$ for CO and U for AF, as elaborated in Appendix B, and this explains the different extent of the two regions. In the antiadiabatic limit, where the HH model

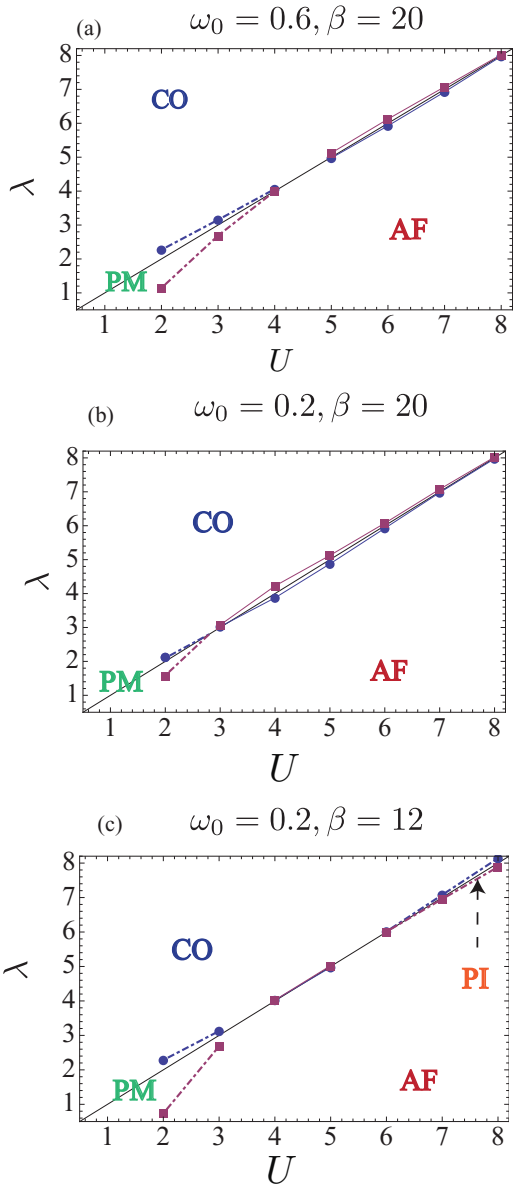

FIG. 10. (Color online) Finite-temperature phase diagram in the U-λ plane. PI stands for a paramagnetic insulating state. Colored dotted lines represent the boundary between a paramagnetic phase and ordered phases, which is continuous. Solid lines show the boundary of the region where the stable solution for CO or AF exists. Red lines shows the boundary of AF, and blue lines indicate the boundary for CO.

becomes the Hubbard model with interaction $U_{\rm eff}$, the T_c (black curves in Fig. 2) translates to T_N on the $-U_{\rm eff} < 0$ side, so that a paramagnetic metallic phase should exist between AF and CO at finite T. Reference 27 points out that the physics in this limit shows up in the weak-coupling regime as a continuous transition between AF and CO. In that sense, the present result is consistent with Ref. 27. However, we note that the Hubbard model cannot explain the difference in the extent of the PM region between $U > \lambda$ and $U < \lambda$ since the Hubbard model solution should be symmetric around the line $U = \lambda$. In addition, we also point out that the region of PM increases as ω_0 increases [compare Figs. 10(a) and 10(b)], which may be

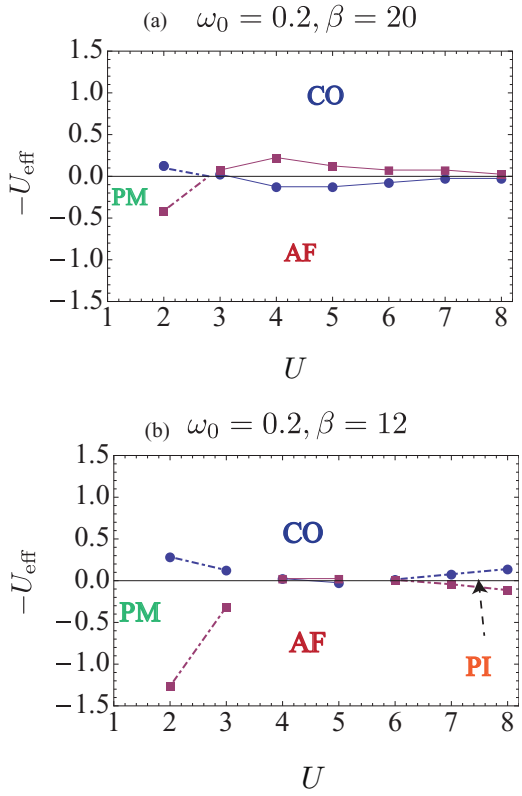

FIG. 11. (Color online) Finite-temperature phase diagram in the plane of U and $-U_{\rm eff}$. Colored dotted lines represent the boundary between a paramagnetic phase and ordered phases (continuous phase transition). Solid lines show the boundary of the region where the stable solution for CO or AF exists. Red lines show the boundary of AF, and blue lines indicate the boundary for CO.

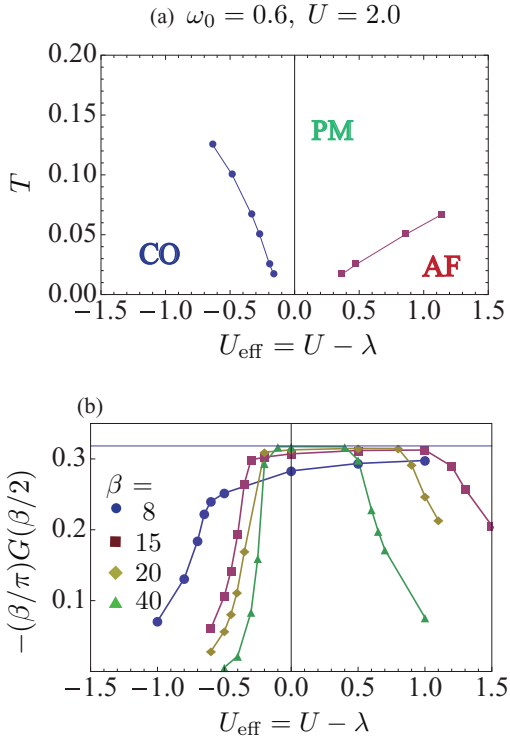

FIG. 12. (Color online) (a) Phase diagram at $U = 2, \omega_0 = 0.6$. (b) $-\frac{\beta}{\pi}G(\tau = \beta/2)$ [a measure of the spectral function $A(\omega = 0)$] against $U_{\rm eff}$ for several temperatures with fixed $\mu = 1, U = 2, \omega_0 = 0.6$. The blue horizontal line shows the bare density of states $1/\pi$.

because the cancellation between the instantaneous repulsive interaction and the retarded interaction is more direct for larger ω_0. Figure 12(a) displays the phase diagram in the plane of T and $U_{\rm eff}$ in the weak-coupling regime, and shows how the PM state between AF and CO behaves towards $T = 0$. We find that the transition temperatures of CO and AF rise much faster as a function of $|U_{\rm eff}|$ than in the case of the Hubbard model ($\omega_0 \to \infty$). Then, the PM region shrinks as the temperature decreases. As for the relation between our results and previous works, which claim either a direct continuous transition between CO and AF at $T = 0$ (Refs. 26 and 27) or the existence of an intermediate PM phase,[17] we cannot judge from our results which scenario is correct. While the extrapolatio of the data in Fig. 12(a) may suggest a finite PM regime at $T = 0$, the phase boundaries for CO and AF may be convex, as suggested by static mean-field theory, so that we cannot draw a definite conclusion on whether a direct continuous phase transition occurs between AF and CO at $T = 0$ or a narrow PM region remains between CO and AF at $T = 0$. Still, our results seem to suggest that a discontinuous direct transition between CO and AF is unlikely to occur at $T \to 0$ and that the behavior of the ground state is qualitatively different from that in the stronger-coupling regime.

In the intermediate-coupling regime, the transition between AF and CO is of first order and takes place within the hysteretic region, which is shown as the region surrounded by red and blue solid lines in Figs. 10 and 11. This coexistence region of two solutions (AF and CO) is located near $U \sim \lambda$ and decreases as the temperatures increases. This result agrees with previous results at $T = 0$.[26,27] We also find that in the strong-coupling regime, the hysteretic region becomes narrower with larger U (or λ) [Figs. 10(a), 10(b), and 11(a)]. In the large-U regime, the CO and AF solutions are separated by a paramagnetic insulating phase [Figs. 10(c) and 11(b)].

Finally, we show evidence for the metallic nature of the PM phase in the small-U regime and the behavior of the density of states at the Fermi level. We use the relation between the Green's function on the imaginary axis and the spectral function [$A(\omega) = -(1/\pi)\mathrm{Im}G_{\rm loc}(\omega)$],

$$G(\tau = \beta/2) = -\int d\omega \frac{1}{2\cosh(\beta\omega/2)} A(\omega). \qquad (24)$$

If the temperature is low enough, $1/\cosh(\beta\omega/2)$ has a strong peak at $\omega = 0$. Then the value of $-(\beta/\pi)G(\tau = \beta/2)$ gives a good estimate of the value of the spectral function $A(\omega = 0)$. The result, shown in Fig. 12(b) for $U = 2$, $\mu = 1$, $\omega_0 = 0.6$, indicates that there is indeed a significant density of states at the Fermi level in the PM phase. Note that we can only observe a small value of $-(\beta/\pi)G(\tau = \beta/2)$ in the paramagnetic state in the strong-coupling regime, so this phase must be regarded as a paramagnetic insulating phase. The value of $-(\beta/\pi)G(\tau = \beta/2)$ monotonically increases and saturates towards the bare density of states, $\rho_0(\omega = 0) = 1/\pi t$, at low enough temperatures, even though the region of PM itself is strongly suppressed. Note that an increase of $-(\beta/\pi)G$ has

also been observed in the analysis of the two-dimensional Holstein-Hubbard model.[17]

IV. CONCLUSION

We have systematically investigated the effect of the electron-electron interaction and the electron-phonon coupling on the ordered states of the half-filled Holstein-Hubbard model, using DMFT and CT-QMC. In the study of the superconducting state, we have found that the interplay of the Coulomb interaction and the retarded attractive interaction leads to a nontrivial structure in the anomalous Green's functions, and we have shown that the maximum transition temperature decreases as a result of the retardation or the Coulomb interaction and shifts to the small U_{eff} regime. The superconducting order parameter shows a similar behavior. We have explained these observations with an effective static model derived from a Lang-Firsov decoupling and a projection onto the zero-boson subspace, and we have investigated the accuracy and reliability of the effective model. Then, we discussed the region where a SC state can be realized in the HH model in the T_c versus U_{eff} phase diagram. We have revealed the effect of the electron-electron and electron-phonon coupling on the gap in the spectral function, and we have pointed out that the retardation or the Coulomb interaction leads to deviations from BCS theory predictions but that if $|U_{\text{eff}}|$ is small enough, the BCS results are recovered. Finally, we have investigated the HH model at $T > 0$ around $U_{\text{eff}} = 0$, allowing for SC, AF, and CO phases. A PM appears between CO and AF in the weak-coupling region, and a paramagnetic insulating phase appears for strong enough coupling, while in the intermediate-coupling regime, the transition between CO and AF is direct and discontinuous and a hysteresis region of AF and CO is located around $U_{\text{eff}} = 0$ at nonzero temperatures.

ACKNOWLEDGMENTS

The authors would like to thank T. Kariyado, T. Oka, M. Tezuka, and A. Koga for constructive advice and discussions. The simulations in this study have been performed using some of the ALPS libraries (Ref. 45). H.A. has been supported by LEMSUPER (EU-Japan Superconductor Project) from JST. PW acknowledges support from SNF Grant 200021-140648.

APPENDIX A: SC AND AF GREEN'S FUNCTIONS

When the system has a gap, the value of Green's functions around $\tau = \beta/2$ becomes very small at low temperatures, which provides a challenge for the CT-QMC measurement. The error bars of the Monte Carlo estimate may become much larger than the exponentially small mean value. Especially in the case of the strong-coupling CT-QMC method, this noise problem is rather severe, providing one of the main drawbacks of an otherwise very flexible and powerful approach. While in the present work we have chosen parameters (temperatures) where these errors are under control and do not cause a problem, we can make an interesting observation here on this issue: the measurement of the SC order parameter has a significantly less severe noise problem than the measurement

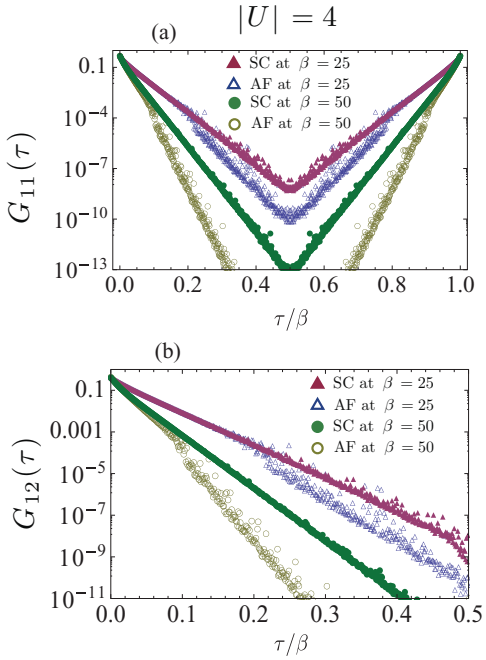

FIG. 13. (Color online) Comparison between SC and AF Green's functions measured after one DMFT iteration at $|U| = 4$, related through Eqs. (A1) and (A2).

of the AF order parameter, so Green's function values as small as 10^{-10} can be accurately measured in the SC (while in the AF the accuracy is limited to about 10^{-5}).

To demonstrate this, we compare a result for the SC in an attractive model with that for the AF in a repulsive one at half filling. The Hubbard model (on a bipartite lattice) with a repulsive U at half filling can be transformed into the model with an attractive interaction $-U$ at half filling (Shiba transformation). The corresponding local Green's functions in the SC and AF phases are related by

$$G_{11}(i\omega_n) = G_{22}(i\omega_n) = \frac{G_{A\uparrow}(i\omega_n) + G_{A\downarrow}(i\omega_n)}{2} = \frac{G_{B\uparrow}(i\omega_n) + G_{B\downarrow}(i\omega_n)}{2}, \tag{A1}$$

$$G_{12}(i\omega_n) = G_{21}(i\omega_n) = \frac{G_{A\uparrow}(i\omega_n) - G_{A\downarrow}(i\omega_n)}{2} = \frac{G_{B\downarrow}(i\omega_n) - G_{B\uparrow}(i\omega_n)}{2}. \tag{A2}$$

Using these equations to derive $G_{11}(i\omega_n)$, $G_{12}(i\omega_n)$ from $G_{A\uparrow}$, $G_{A\downarrow}$, we compare the measurements in the SC and AF phases in Figs. 13 and 14. In all calculations, we start from the static mean-field theory (BCS) solution, and we fixed the CPU time for each DMFT iteration to 12 min on 16 CPUs. Figures 13(a) and 13(b) show $G_{11}(i\omega_n)$ and $G_{12}(i\omega_n)$, respectively, after the first iteration, while Fig. 14 shows the fully converged results after 50 iterations. As can be seen, the measurement in the SC phase suffers from less noise and provides an accurate estimate of the Green's function even around $\tau = \beta/2$. This result is reminiscent of an observation by Hirsch[46] that in quantum Monte Carlo simulations of

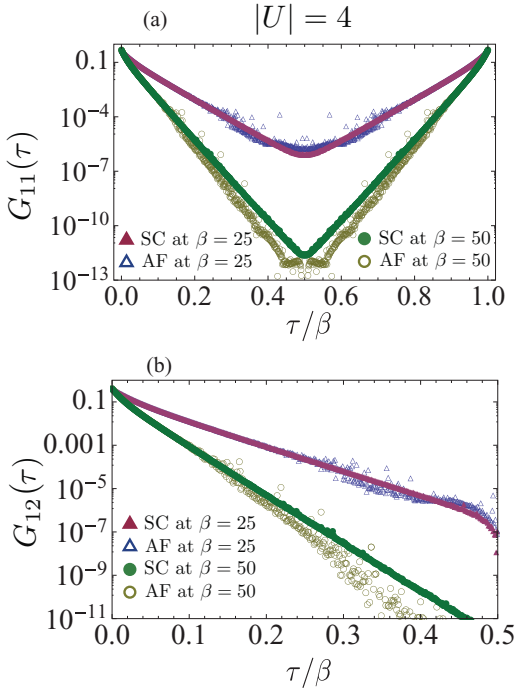

FIG. 14. (Color online) Comparison between fully converged SC and AF Green's functions measured after 50 DMFT iterations at $|U| = 4$, related through Eqs. (A1) and (A2).

the Hubbard model, the accuracy of spin-spin correlations measured in the z or x direction can be very different.

APPENDIX B: STATIC MEAN-FIELD TREATMENT FOR AF AND CO

In order to gain some insights into the behavior of the CO and AF phases, we briefly discuss a static mean-field theory for the HH model.[27] We treat both interactions in Eq. (1) with a mean-field approximation by introducing the average of the lattice displacement $\langle b_i^\dagger + b_i\rangle/\sqrt{2\omega_0}$ and the averaged density $\langle n_{i,\sigma}\rangle$. The mean-field Hamiltonian is decomposed as

$$H_{\rm MF} \equiv H^e_{\rm MF} + H^{ph}_{\rm MF}, \tag{B1}$$

where

$$H^e_{\rm MF} = -t\sum_{\langle i,j\rangle,\sigma}[c^\dagger_{j,\sigma}c_{i,\sigma} + {\rm H.c.}] + \sum_i [U(\langle n_{i\uparrow}\rangle n_{i\downarrow} + \langle n_{i\downarrow}\rangle n_{i\uparrow}) - \mu n_i + g\langle b_i^\dagger + b_i\rangle n_i] \tag{B2}$$

and

$$H^{ph}_{\rm MF} = g\sum_i (b_i^\dagger + b_i)(\langle n_i\rangle - 1) + \omega_0\sum_i b_i^\dagger b_i. \tag{B3}$$

From $H^{ph}_{\rm MF}$, we find $\langle b_i\rangle = \langle b_i^\dagger\rangle = -\frac{g}{\omega_0}(\langle n_i\rangle - 1)$. Then we obtain

$$H^e_{\rm MF} = -t\sum_{\langle i,j\rangle,\sigma}[c^\dagger_{j,\sigma}c_{i,\sigma} + {\rm H.c.}] - \sum_i(\mu-\lambda)n_i + \sum_{i,\sigma} n_{i\sigma}(U\langle n_{i\bar\sigma}\rangle - \lambda\langle n_i\rangle). \tag{B4}$$

This Hamiltonian shows that the effective attractive interaction $-n_{i\sigma}\lambda\langle n_i\rangle$ comes from electrons of both spins, which is different from the case of the Hubbard interaction. In the following, let us focus on half filling and consider the solution of CO and AF.

For CO, $\langle n_{A\uparrow}\rangle = \langle n_{A\downarrow}\rangle \neq \langle n_{B\uparrow}\rangle = \langle n_{B\downarrow}\rangle$, and we define the order parameter as $\Phi_{\rm CO} = (\langle n_{A\uparrow}\rangle - \langle n_{B\uparrow}\rangle)/2$. On the other hand, for AF, $\langle n_{A\uparrow}\rangle = \langle n_{B\downarrow}\rangle \neq \langle n_{A\downarrow}\rangle = \langle n_{B\uparrow}\rangle$, and we define the order parameter as $\Phi_{\rm AF} = (\langle n_{A\uparrow}\rangle - \langle n_{A\downarrow}\rangle)/2$. Then we obtain a self-consistent equation,

$$1 = V\int d\xi\rho(\xi)\frac{\tanh[\beta E(\xi,\Phi,V)/2]}{2E(\xi,\Phi,V)}, \tag{B5}$$

where $\rho(\xi)$ is the density of states for bare electrons and $E(\xi,\Phi,V) = \sqrt{V^2\Phi^2 + \xi^2}$. For CO we put $\Phi = \Phi_{\rm CO}, V = |U - 2\lambda|$, and for AF, we set $\Phi = \Phi_{\rm AF}, V = |U|$.

Note that if we consider CO and SC in the attractive Hubbard model within the static mean-field approximation, we put $V = |U| = |U_{\rm eff}|$ in Eq. (B5). On the other hand, when we consider the Holstein model, we use $V = 2|\lambda| = 2|U_{\rm eff}|$, which corresponds to the effective interaction for both spin up and down. This explains why the transition temperature for CO is enhanced in the small $U_{\rm eff}$ regime as ω_0 decreases, as was pointed out in Refs. 41 and 42.

We also note that the static mean-field analysis can explain the reason why the PM region is larger on the $U > \lambda$ side than on the $U < \lambda$ side. This comes from the different dependences of AF and CO on U and λ. At a given temperature T, let $V_0 > 0$ satisfy

$$1 = V_0\int d\xi\rho(\xi)\frac{\tanh[\beta E(\xi,0,V_0)/2]}{2E(\xi,0,V_0)}. \tag{B6}$$

The mean-field analysis then dictates that the boundary of CO and PM is located at $\lambda = (V_0 + U)/2$, while the boundary of AF and PM is at $U = V_0$. The two boundaries cross at $U = \lambda = V_0$, and a first-order transition occurs for $U, \lambda > V_0$.

[1] A. Lanzara, P. V. Bogdanov, X. J. Zhou, S. A. Kellar, D. L. Feng, E. D. Lu, T. Yoshida, H. Eisaki, A. Fujimori, K. Kishio, J. I. Shimoyama, T. Noda, S. Uchida, Z. Hussain, and Z. X. Shen, Nature (London) **412**, 510 (2001).

[2] Y. Takabayashi, A. Y. Ganin, P. Jeglic, D. Arcon, T. Takano, Y. Iwasa, Y. Ohishi, M. Takata, N. Takeshita, K. Prassides, and M. J. Rosseinsky, Science **323**, 1585 (2009).

[3] M. Capone, M. Fabrizio, C. Castellani, and E. Tosatti, Rev. Mod. Phys. **81**, 943 (2009).

[4] O. Gunnarsson, Rev. Mod. Phys. **69**, 575 (1997).

[5] T. Kato, T. Kambe, and Y. Kubozono, Phys. Rev. Lett. **107**, 077001 (2011).

[6] Y. Kubozono, H. Mitamura, X. Lee, X. He, Y. Yamanari, Y. Takahashi, Y. Kaji, R. Eguchi, K. Akaike, T. Kambe, H. Okamoto, A. Fujiwara, T. Kato, T. Kosugi, and H. Aoki, Phys. Chem. Chem. Phys. **13**, 16476 (2011).

[7] T. Kosugi, T. Miyake, S. Ishibashi, R. Arita, and H. Aoki, Phys. Rev. B **84**, 214506 (2011).

[8] A. Subedi and L. Boeri, Phys. Rev. B **84**, 020508(R) (2011).
[9] Y. Nomura, K. Nakamura, and R. Arita, Phys. Rev. B **85**, 155452 (2012).
[10] M. Tezuka, R. Arita, and H. Aoki, Phys. Rev. Lett. **95**, 226401 (2005); Phys. Rev. B **76**, 155114 (2007).
[11] H. Fehske, G. Hager, and E. Jeckelmann, Europhys. Lett. **84**, 57001 (2008).
[12] R. T. Clay and R. P. Hardikar, Phys. Rev. Lett. **95**, 096401 (2005).
[13] E. Berger, P. Valasek, and W. von der Linden, Phys. Rev. B **52**, 4806 (1995).
[14] A. Macridin, B. Moritz, M. Jarrell, and T. Maier, Phys. Rev. Lett. **97**, 056402 (2006).
[15] E. Khatami, A. Macridin, and M. Jarrell, Phys. Rev. B **78**, 060502(R) (2008).
[16] S. Kumar and J. van den Brink, Phys. Rev. B **78**, 155123 (2008).
[17] E. A. Nowadnick, S. Johnston, B. Moritz, R. T. Scalettar, and T. P. Devereaux, Phys. Rev. Lett. **109**, 246404 (2012).
[18] W. Metzner and D. Vollhardt, Phys. Rev. Lett. **62**, 324 (1989).
[19] A. Georges and G. Kotliar, Phys. Rev. B **45**, 6479 (1992).
[20] A. Georges, G. Kotliar, W. Krauth, and M. J. Rozenberg, Rev. Mod. Phys. **68**, 13 (1996).
[21] P. Werner and A. J. Millis, Phys. Rev. Lett. **99**, 146404 (2007).
[22] W. Koller, D. Meyer, Y. Ono, and A. C. Hewson, Europhys. Lett. **66**, 559 (2004).
[23] G. Sangiovanni, M. Capone, C. Castellani, and M. Grilli, Phys. Rev. Lett. **94**, 026401 (2005).
[24] W. Koller, A. C. Hewson, and D. M. Edwards, Phys. Rev. Lett. **95**, 256401 (2005).
[25] J. K. Freericks and M. Jarrell, Phys. Rev. Lett. **75**, 2570 (1995).
[26] J. Bauer, Europhys. Lett. **90**, 27002 (2010).
[27] J. Bauer and A. C. Hewson, Phys. Rev. B **81**, 235113 (2010).
[28] J. Bauer, J. E. Han, and O. Gunnarsson, Phys. Rev. B **84**, 184531 (2011).
[29] J. Bauer, J. E. Han, and O. Gunnarsson, Phys. Rev. B **87**, 054507 (2013).
[30] A. B. Migdal, Sov. Phys. JETP **7**, 996 (1958).
[31] G. M. Eliashberg, Sov. Phys. JETP **11**, 696 (1960); **12**, 1000 (1961).
[32] P. Morel and P. W. Anderson, Phys. Rev. **125**, 1263 (1962).
[33] W. L. McMillan, Phys. Rev. **125**, 331 (1968).
[34] M. Casula, P. Werner, L. Vaugier, F. Aryasetiawan, T. Miyake, A. J. Millis, and S. Biermann, Phys. Rev. Lett. **109**, 126408 (2012).
[35] J. T. Devreese and A. S. Alexandrov, Rep. Prog. Phys. **72**, 066501 (2009).
[36] A. S. Alexandrov and N. F. Mott, Rep. Prog. Phys. **57**, 1197 (1994).
[37] P. Werner, A. Comanac, L. de'Medici, M. Troyer, and A. J. Millis, Phys. Rev. Lett. **97**, 076405 (2006).
[38] E. Gull, A. J. Millis, A. I. Lichtenstein, A. N. Rubtsov, M. Troyer, and P. Werner, Rev. Mod. Phys. **83**, 349 (2011).
[39] I. G. Lang and Y. A. Firsov, Sov. Phys. JETP **16**, 1301 (1962).
[40] For the attractive Hubbard model, the treatment of the superconducting phase within DMFT and the hybridization expansion CT-QMC approach has been discussed in Ref. 43.
[41] J. K. Freericks, M. Jarrell, and D. J. Scalapino, Europhys. Lett. **25**, 37 (1994).
[42] J. K. Freericks, M. Jarrell, and D. J. Scalapino, Phys. Rev. B **48**, 6302 (1993).
[43] A. Koga and P. Werner, Phys. Rev. A **84**, 023638 (2011).
[44] G. Sangiovanni, A. Toschi, E. Koch, K. Held, M. Capone, C. Castellani, O. Gunnarsson, S.-K. Mo, J. W. Allen, H.-D. Kim, A. Sekiyama, A. Yamasaki, S. Suga, and P. Metcalf, Phys. Rev. B **73**, 205121 (2006).
[45] A. Albuquerque *et al.*, J. Magn. Magn. Mater. **310**, 1187 (2007); B. Bauer *et al.*, J. Stat. Mech. Theor. Exp. (2011) P05001.
[46] J. E. Hirsch, Phys. Rev. B **35**, 1851 (1987).